

## **PLASMA AND MHD CONTROL OF OBLIQUE SHOCKS**

**Sergey O. Macheret, Mikhail N. Shneider, Sohail H. Zaidi, Richard B. Miles**

Princeton University [macheret@princeton.edu](mailto:macheret@princeton.edu)

**and David M. Van Wie**

Johns Hopkins University Applied Physics Laboratory

The paper reviews recent studies of supersonic/hypersonic flow and shock wave control using plasma energy addition and magnetohydrodynamics (MHD), focusing on the work by the Princeton University group and their collaborators. Applications include sonic boom mitigation and optimization of scramjet inlets. Experimental and computational studies of interaction of oblique shocks with laser-generated blast wave and thermal wake demonstrate the possibility of shock mitigation in a repetitive-pulse mode. Analysis of interaction parameter for MHD control of cold hypersonic flows with external ionization shows that significant interaction can be achieved with energy-efficient ionization by electron beams. The maximum achievable interaction parameter sharply increases with increasing Mach number and altitude; however, interelectrode arcing may limit the performance. For MHD control of scramjet inlets, nonequilibrium electrical conductivity is created by electron beams injected into the gas along magnetic field lines. At Mach numbers higher than the design value, the shocks that would otherwise enter the inlet can be moved back to the cowl lip by a short MHD generator at the first compression ramp. To increase air capture at Mach numbers below the design value, a heated region is used to create a “virtual cowl” and to deflect flow streamlines into the inlet. The best location of the energy addition region is near the intersection of the nose shock of the vehicle with the continuation of the cowl line, and slightly below that line. Stretching and tilting the energy addition region improves performance. By spending only a few percent of the enthalpy flux into the inlet, the air capture and engine thrust can be increased by 15-20%, with no loss in specific impulse.

### **1. Introduction**

Report Documentation Page				Form Approved OMB No. 0704-0188	
Public reporting burden for the collection of information is estimated to average 1 hour per response, including the time for reviewing instructions, searching existing data sources, gathering and maintaining the data needed, and completing and reviewing the collection of information. Send comments regarding this burden estimate or any other aspect of this collection of information, including suggestions for reducing this burden, to Washington Headquarters Services, Directorate for Information Operations and Reports, 1215 Jefferson Davis Highway, Suite 1204, Arlington VA 22202-4302. Respondents should be aware that notwithstanding any other provision of law, no person shall be subject to a penalty for failing to comply with a collection of information if it does not display a currently valid OMB control number.					
1. REPORT DATE <b>20 OCT 2003</b>		2. REPORT TYPE <b>N/A</b>		3. DATES COVERED <b>-</b>	
4. TITLE AND SUBTITLE <b>Plasma And Mhd Control Of Oblique Shocks</b>				5a. CONTRACT NUMBER	
				5b. GRANT NUMBER	
				5c. PROGRAM ELEMENT NUMBER	
6. AUTHOR(S)				5d. PROJECT NUMBER	
				5e. TASK NUMBER	
				5f. WORK UNIT NUMBER	
7. PERFORMING ORGANIZATION NAME(S) AND ADDRESS(ES) <b>Princeton University; Johns Hopkins University Applied Physics Laboratory</b>				8. PERFORMING ORGANIZATION REPORT NUMBER	
9. SPONSORING/MONITORING AGENCY NAME(S) AND ADDRESS(ES)				10. SPONSOR/MONITOR'S ACRONYM(S)	
				11. SPONSOR/MONITOR'S REPORT NUMBER(S)	
12. DISTRIBUTION/AVAILABILITY STATEMENT <b>Approved for public release, distribution unlimited</b>					
13. SUPPLEMENTARY NOTES <b>See also ADM001739, Thermochemical processes in plasma aerodynamics (Conference Proceedings, 28-31 July 2003 (CSP 03-5031)., The original document contains color images.</b>					
14. ABSTRACT					
15. SUBJECT TERMS					
16. SECURITY CLASSIFICATION OF:			17. LIMITATION OF ABSTRACT <b>UU</b>	18. NUMBER OF PAGES <b>38</b>	19a. NAME OF RESPONSIBLE PERSON
a. REPORT <b>unclassified</b>	b. ABSTRACT <b>unclassified</b>	c. THIS PAGE <b>unclassified</b>			

### 3 Workshop “Thermochemical processes in plasma aerodynamics”

Energy addition for modification of the external flow field around a vehicle is a well known technique and, primarily, has been studied and used to reduce the drag on objects flying at supersonic speeds. Historically, energy addition in the supersonic flow was proposed as an alternative technique of reducing drag on a flying object.<sup>1-3</sup>

In principle, with a proper position, shape, and power of the thermal source relative to the external surface of the body, one can substantially decrease its aerodynamic drag and thereby reduce the value of thrust required to maintain the steady flight. Such reasoning was discussed in a number of papers.<sup>1-8</sup> The problem of supersonic flow past a localized region of heat release was treated in Refs. 4-7, 10-12.

In addition to drag reduction, other applications of energy addition to external high-speed flows have been suggested recently. Those include, for example, control of oblique shock waves and optimization of scramjet inlets, control of shock reflection and boundary layer separation, and sonic boom mitigation.

Most recently, Ref. 13 presented an overview of the results of aerodynamic flow control by energy deposition obtained by the Princeton group and their collaborators during the past few years and insufficiently reflected in the recent reviews on this topic.<sup>11, 12</sup> The principal topics included:<sup>13</sup>

- The effect of a plasma (directed-energy) air spike on drag reduction and effective body geometry in hypersonic flows.
- Modeling of “virtual cowl,” i.e., of energy addition to hypersonic flow off the vehicle in order to increase air mass capture and reduce spillage in scramjet inlets at Mach numbers below the design value.
- Numerical studies of aerodynamic forces created by off-axis heat addition upstream of a body. These forces and moments can be used for supersonic/hypersonic vehicle steering.
- Experiments and numerical modeling of pulsed off-body energy addition for sonic boom mitigation.

In the present paper, we briefly review just two of the listed energy addition topics: the “virtual cowl” concept, and sonic boom mitigation by energy addition.

The issue of magnetohydrodynamic (MHD) control of hypersonic flows is being extensively studied for applications in hypersonic airbreathing propulsion. Indeed, the geometry, size, and weight of scramjet-powered hypersonic vehicles are largely dictated by the need to compress the ambient low-density air upstream of the combustor.<sup>14</sup> The optimum geometry corresponds to the well-known shock-on-lip (SOL) condition: the compression ramp shocks converge on the cowl lip, and the reflected shock impinges on the inlet shoulder.<sup>14</sup> At Mach

### 3 Workshop “Thermochemical processes in plasma aerodynamics”

numbers higher than the design value, the shocks move inside the inlet, causing local hot spots, loss of stagnation pressure, possible boundary layer separation, and engine unstart. At Mach numbers lower than the design value, a portion of the air compressed by the shock misses the inlet (“spillage”), resulting in thrust decrease.

To avoid performance penalties at off-design Mach numbers, a variable geometry inlet can be used. An alternative approach is to optimize inlets using energy addition to or extraction from the flow. Plasmas and magnetohydrodynamic devices may offer viable optimization schemes.<sup>15-</sup>

37

An important factor in MHD control is that in the flight regime of interest, static temperature is too low for thermal ionization of air. Therefore, nonequilibrium ionization in MHD devices must be applied.<sup>15, 28-30, 36-37</sup> The energy cost of ionization imposes very rigid constraints on the choice of ionization methods: only the most energetically efficient ionization method, that by electron beams, can be used in these devices. However, even with the most efficient ionizer, the very existence of ionization cost does not allow the ionization degree and the conductivity in hypersonic MHD devices to be very high.<sup>15, 28-30, 36-37</sup> This makes the task of using MHD for hypersonic flow control and power generation challenging and require careful analysis and optimization.

An attractive scenario for MHD inlet control<sup>15, 28-30, 36-37</sup> is to design the vehicle for a relatively low Mach number (for example, Mach 5 or 6), and, at high Mach numbers, move the shocks from inside the inlet back to the cowl lip by an MHD generator device placed at one of the compression ramps. The advantages of this method are the following: 1) the vehicle size and weight can be reduced due to both absence of a mechanically variable inlet and the shortening of the compression ramp (the weight savings may offset the weight of the magnet and other MHD-related hardware); 2) no net power is required to run the MHD device, since the generator mode is used, and the power requirements for air ionization can be minimized with electron beams as ionizers; 3) flexibility of flow control. A disadvantage of this approach is that the inevitable Joule heating and other dissipative processes result in some stagnation pressure losses.

In our recent work,<sup>15, 28-30, 36-37</sup> we analyzed inlet control at Mach numbers higher than the design value by means of an on-ramp MHD generator. The principal new element in the most recent work<sup>36,37</sup> is that MHD regions are very short compared with both length and width of the vehicle forebody. In the present paper, we review the results briefly.

In recent papers, we also suggested and analyzed a new concept of increasing the mass capture, dubbed a “virtual cowl”.<sup>15, 35</sup> The essence of the method is to create a heated region upstream of and somewhat below the cowl lip. The incoming flow would be deflected by the

### **3 Workshop “Thermochemical processes in plasma aerodynamics”**

elevated-temperature and/or elevated pressure region, causing an increased mass flow into the inlet. The heated region may be generated by supplying microwave or RF energy to a volume pre-ionized by a focused laser or electron beam. Other possible means include hot gas or plasma jets, and also external combustion. Shooting combustible liquid or solid pellets (see Ref. 21) upstream may be an interesting option. An important advantage of the new method is that the air entering the inlet would have experienced little or no heating. Thus, irreversibilities and stagnation pressure losses associated with heating can be minimized. In this paper, we briefly review the results of computational studies of the virtual cowl concept,<sup>35</sup> and present recently performed assessment of the effects on engine performance.

#### **2. Energy addition in supersonic flows for sonic boom mitigation**

Shock waves generated by a supersonic object are known to produce a sonic boom on the ground. Sonic boom formation has been the main obstacle in the development of commercial supersonic vehicles. For a supersonic aircraft, the near-field shock structure is a complex array of shock waves that originate from various parts of the aircraft. In the far field, these shock waves coalesce and produce an N-shaped pressure signature on the ground. Although the sonic boom is a far-field phenomenon, several near-field techniques have been suggested to attenuate the shocks with the assumption that it will eliminate or partially reduce the sonic boom on the ground. These techniques include the design of exceptionally long aircraft,<sup>38,39</sup> use of underwing thermal gradients,<sup>40</sup> and possibility of high speed oscillations of flight velocity.<sup>41</sup> Current work focuses mainly on the development of long, thin aircraft because the other methods seem unrealistic due to practical considerations. Energy addition is an alternative approach to sonic boom mitigation. It has been argued that upstream energy addition to a supersonic vehicle may weaken the shock wave and may prove to be a useful approach to suppress the sonic boom on the ground. Recent work related to DARPA’s Quiet Supersonic Platform Program, which was conducted at Princeton, addressed these issues in some detail. The details of this project have been presented by Miles et. al.<sup>42</sup> The results indicated that steady state off-body energy addition can reduce the far-field signature primarily by suppressing the far-field coalescence of the shock waves originating from the various parts of the vehicle.<sup>42</sup>

The dynamic effects of energy addition were investigated with a time-marching Euler code based on 2<sup>nd</sup> order MacCormack method on rectangular grid. Preliminary modeling was performed in two dimensions with the energy added along a line across the two-dimensional domain and the effects seen on the shock structure from a wedge. The simplicity of this configuration allows the code to follow the dynamics of the interaction of the energy addition

### 3 Workshop “Thermochemical processes in plasma aerodynamics”

with the bow shock. An example of the interaction of a series of energy addition pulses is shown in Fig. 1. These are five frames from a ‘movie’ that show the dynamics of the interaction. Fig. 2 shows the impact of those pulses on the pressure measured at the bottom of the frames shown in Fig. 2 ( $z = -1.6\text{m}$ ).

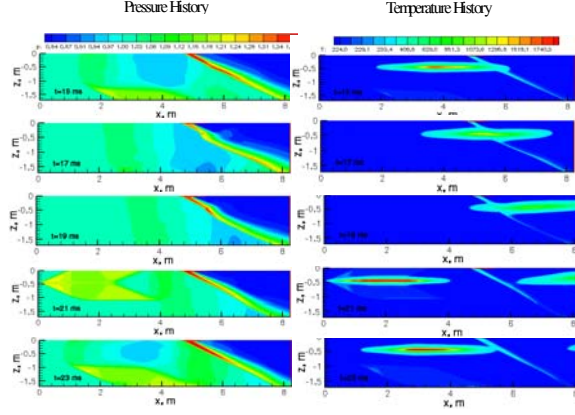


**Fig. 1.** Two-dimensional, time-accurate model of pulsed energy addition. Flow is from left to right. The energy addition regime modulates and weakens the bow shock

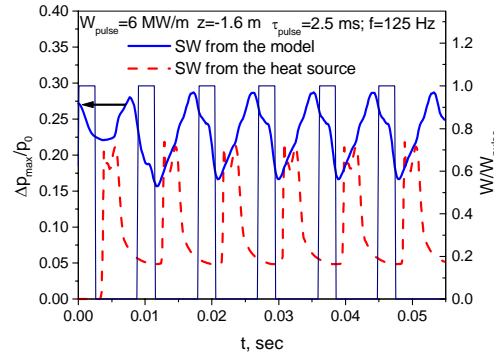


**Fig. 2.** Maximum relative pressures at the bottom cross section:  $z=-1.6\text{ m}$  on Fig. 1. Rectangles show the energy addition pulses in relative units. The bow shock pressure is modulated in time (solid line), but averaged pressure amplitude from the bow shock is 20% lower than steady-state one without the heat addition (shown by the arrow). The pressure associated with the shock generated by the heat addition is shown by the dotted line and maximal pressure from the heat source is significantly lower than one from the model. Pulse duration  $\tau_{\text{pulse}} = 2.5\text{ ms}$ ; frequency  $f=125\text{ Hz}$ .

In the absence of energy addition, the bow shock produces a  $P_{\text{max}}/P_0$  of 0.027 which is shown by the arrow on the left side of Fig. 2. In the presence of the pulsed energy addition, the  $P_{\text{max}}/P_0$  from the bow shock oscillates, but is consistently lower in value than it is in the absence of the energy addition. The average reduction in bow shock strength is about 20%. The energy addition process itself generates an oscillating shock, but that is significantly weaker, as shown by the

### 3 Workshop “Thermochemical processes in plasma aerodynamics”

dotted line. It is expected that the addition of energy by pulses such as this will reduce the total power requirements for modifying the far-field signature, and it may introduce new effects that further suppress the far-field coalescence and reduce sonic boom. These dynamic far-field effects cannot yet be predicted and have not yet been measured.<sup>42</sup>

The above example explicitly demonstrates the significance of energy addition to control flow fields around objects flying at supersonic speeds. Among various methods of energy addition, laser initiated optical discharges have been found to be an efficient way to control the position and structures of shock waves.<sup>11-13, 43-45</sup> In this regard, laser based energy addition techniques can find an important application to sonic boom mitigation. To demonstrate this approach and to investigate the dynamic effects of energy addition upstream of the shock wave produced by a model in the flow, experiments were performed under DARPA’s Quiet Supersonic Platform program at Princeton.

The experimental program was established to validate model predictions for the dynamic energy addition and to examine the real time near-field interaction of the energy addition with the shock wave produced in the flow. A Mach 2.4 nozzle was designed to perform experimental studies. A model was placed in the test section [length=6", width=2.15", height=1.9"] to produce a shock wave. The static pressure in the test section was near atmospheric to permit localized energy addition by laser induced breakdown. A 10 Hz Nd:YAG laser was employed to add energy into the flow. The pulse energy was about 350 mJ/pulse, and a 100 mm focal length was used to obtain a breakdown in the region of interest upstream of the model. A Princeton Scientific Instrument ultra-fast framing camera (PSI-4) was used to capture the shock wave interactions in the test section as the energy is added to the flow. Fig. 3 shows the experimental shadowgraph images captured with the desired flow in the tunnel. Flow is from left to right, and the laser was focused at the position mentioned in Fig. 3. The frame integration time was 2  $\mu$ s. Frames in Fig. 3 clearly show the thermal spot along with its associated shock wave propagating with the flow. As the thermal spot passes through the oblique shock, a significant distortion and weakening of the shock can be seen in frames 4 to 7. Full details on these experiments can be found in Ref. 43. It is important to note that for an effective sonic boom reduction, the position of the laser breakdown spot should be optimized so that the shock wave generated by the thermal spot weakens before it reaches the bow shock. In this case, the interaction of the thermal spot would have a more pronounced impact on the bow shock.

### 3 Workshop “Thermochemical processes in plasma aerodynamics”

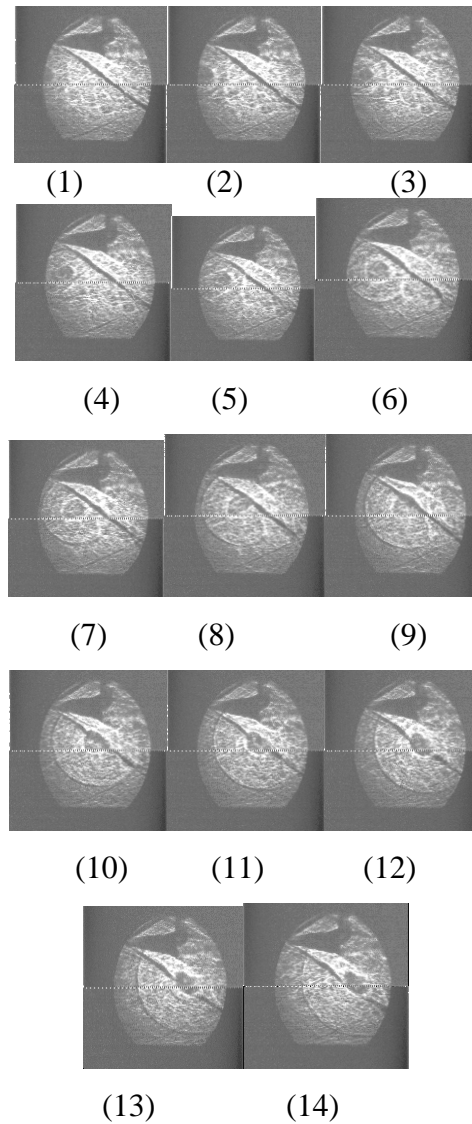


**Fig. 3.** Shadowgraph images of the interaction between the laser thermal spot and blast wave and the oblique shock wave from a wedge in a Mach 2.4 flow. Images are 4  $\mu$ s apart.

Modeling was conducted at the flow conditions used for the experimental studies ( $M=2.4$ ,  $P_0=1$  atm,  $T_0=136$  K,  $\gamma=1.4$ ). A time marching two dimensional Euler code was used for this purpose. The energy deposition region was assumed to have a cylindrical shape and a Gaussian distribution in the (x,y) plane with an effective radius of 0.125 cm. This assumption was based on the fact that a laser spark produces a cylindrical shock wave and a rarefied thermal spot that both move downstream with the flow.

Fig. 4 presents the computational results describing the dynamics of interaction of the energy addition with the shock wave generated by the model. The energy addition itself

### 3 Workshop “Thermochemical processes in plasma aerodynamics”

generates a shock wave that grows as it propagates in the flow. Frames in Fig. 4 clearly show the complex interaction of the entropy spot with the oblique shock and also show attenuation of the shock wave as it passes through the entropy spot. Fig. 4 also shows the way the laser generated shock wave gets reflected from the model surface, which makes the dynamics of interaction even more complex.

Calculations were performed for the interaction of the flow-convected thermal spot with and without the accompanying shock wave with the oblique shock from the model. A remarkable difference between the two cases can be seen in terms of pressure variation along the surface of the test section, as shown in Figure 5. In the case when the laser spot is focused 10 mm upstream and 10 mm below the model, the pressure variation is maximum. The rise in pressure is due to the interaction of the shock wave surrounding the thermal spot with the oblique shock wave, whereas the pressure decreases when the thermal spot interacts with the model shock. Since pressure calculations were made in the near field, only 2.5 cm below the model, the interaction of the shock waves with the expansion fan located at the far right edge of the model affects the pressure in a complex fashion. Due to this, several fluctuations in the pressure curve can be seen in Fig. 5. As the laser spark is moved farther away from the model edge (40 mm upstream), the shock wave around the thermal spot becomes weaker and the corresponding pressure variations become smaller in amplitude, as can be seen in Fig.

5. For the isobaric case where the pressure inside the energy deposition region has been assumed constant (thermal spot without the surrounding shock wave), only the interaction of the thermal spot has been analyzed, and the pressure associated with the oblique shock wave, unlike the previous two cases, was reduced without any large fluctuations (Fig. 5). Thus, the position of the laser breakdown spot should play a vital role in the mitigation of shock waves and of the sonic boom from a supersonic vehicle. Far-field experiments will be required to demonstrate the effectiveness of this technique.

### 3 Workshop “Thermochemical processes in plasma aerodynamics”

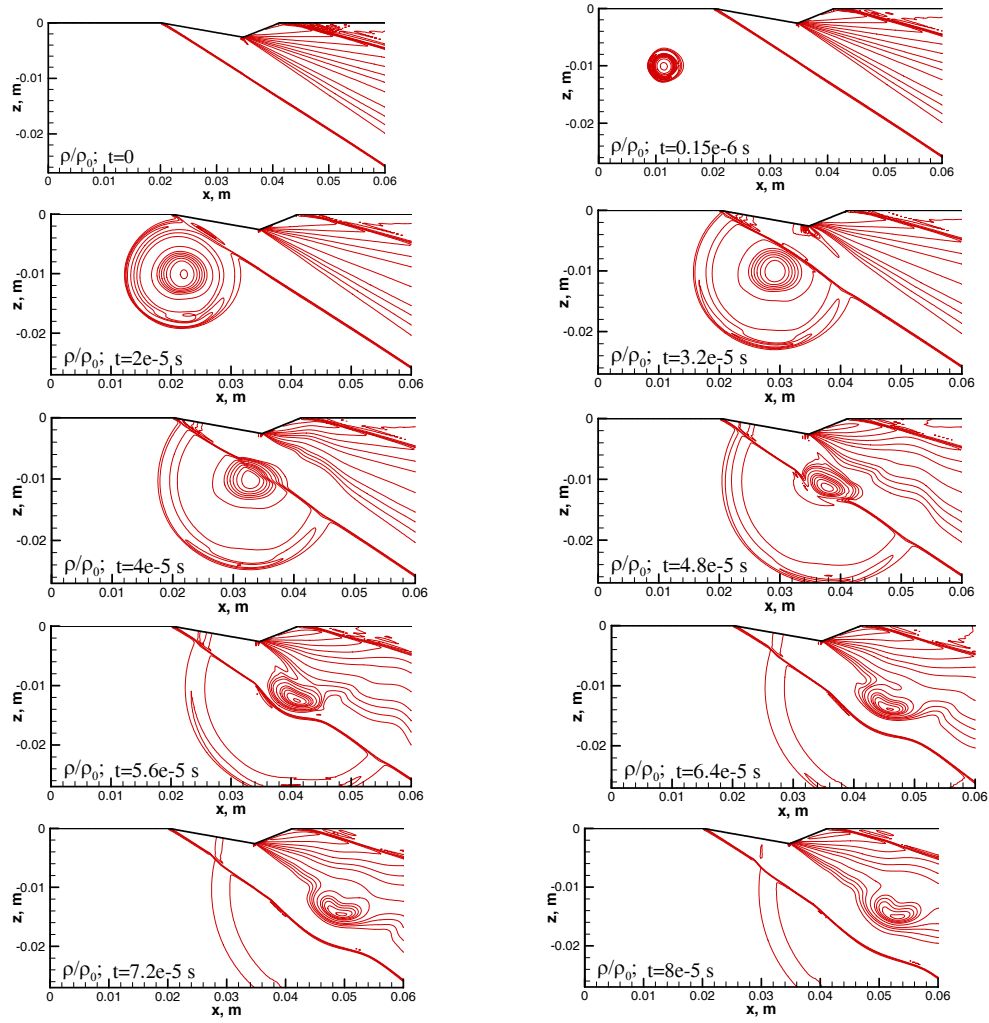


**Fig. 4.** Two dimensional, time accurate model of laser spark and the oblique shock wave interaction (density contours). Flow is from left to right.

### 3 Workshop “Thermochemical processes in plasma aerodynamics”

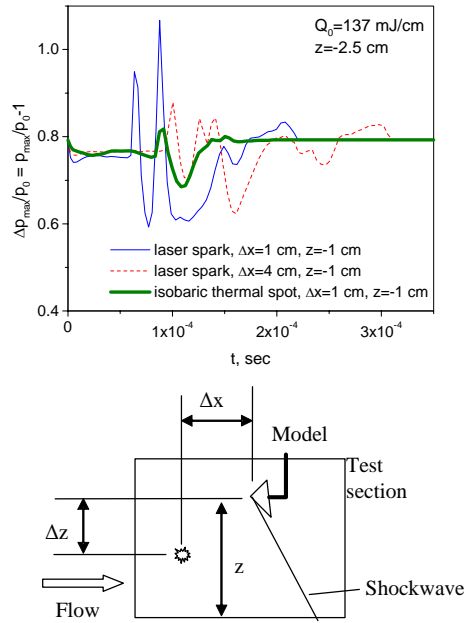


**Fig. 5.** Top – computational predictions of maximum relative pressures at the bottom of the test section for various energy addition positions; bottom – geometry indicating the position for localized energy addition to predict pressure variations at the bottom of the test section

The results of both experiment and numerical modeling clearly demonstrate strong influence of the pulsed power deposition in supersonic flow on shock wave intensity in the near field of the body. But whether the problem of sonic boom mitigation in the far field can be solved by such means requires additional theoretical and experimental investigations. It is possible that the ‘quiet’ power deposition (a long, thin heated region with low power input per unit volume) suggested by Kolesnichenko<sup>46,47</sup> and by Georgievskii and Levin<sup>48</sup> can be useful not only for drag reduction, but also for sonic boom mitigation, because in that case most of the power is spent on creation of the thermal wake, rather than on generating shocks.

#### 1. Basic analysis of MHD flow control in cold hypersonic flows: the interaction parameter<sup>29</sup>

To estimate MHD effects in relatively cold hypersonic flow and boundary layer, the momentum equation for the gas

$$\rho \frac{d\vec{u}}{dt} = -\nabla p + \vec{j} \times \vec{B} + \mu \Delta \vec{u} \quad (1)$$

should be analyzed jointly with other appropriate gas dynamic and plasma kinetic equations, and with the generalized Ohm’s law

### 3 Workshop “Thermochemical processes in plasma aerodynamics”

$$\vec{j} = \sigma \vec{E}^* + \frac{\Omega_e}{B} \vec{j} \times \vec{B} + \frac{\Omega_e \Omega_i}{B^2} (\vec{j} \times \vec{B}) \times \vec{B} \quad (2)$$

where  $\vec{E}^* = \vec{E} + \vec{u} \times \vec{B}$  is the electric field in the reference frame moving with the gas, and  $\Omega_e$  and  $\Omega_i$  are the electron and ion Hall parameters:

$$\Omega_e = \frac{eB}{mk_{en}}; \quad \Omega_i = \frac{eB}{M_n k_{n+} n} \quad (3)$$

The second term in the right-hand side of Eq. (2) represents the Hall effect, and the third term, nonlinear with respect to  $B$ , represents the ion slip. In the analysis, we will disregard negative ions and also assume quasineutrality,  $n_e = n_+ \approx n_-$ .

The MHD interaction parameter, also referred to as the Stuart number,  $S$ , is the ratio of ponderomotive (Ampere) and inertia forces. With ion slip correction,

$$S = \frac{\sigma B^2 L}{(1 + \Omega_e \Omega_i) \rho u} \quad (4)$$

where  $L$  is the length of MHD region. When ion slip is small,  $\Omega_e \Omega_i \ll 1$ , the Stuart number increases with magnetic field as  $B^2$ . However, at very strong magnetic fields and in low-density gases, when  $\Omega_e \Omega_i \gg 1$ , the interaction parameter reaches its asymptotic value independent of  $B$ :

$$S \rightarrow (L/u) k_{n+} n_+ \quad (5)$$

The physical meaning of Eq. (5) is that the maximum ion momentum change occurs when they are essentially stopped by the strong transverse magnetic field, and then momentum transfer from the ions to the gas is limited by the number of collisions of a neutral molecule with ions. Indeed, the right-hand side of Eq. (5) is simply the ratio of the flow residence time in the MHD region to the mean time for a molecule to collide with an ion.

As discussed in our earlier work, at flight Mach numbers up to about Mach 12, thermal ionization cannot provide an adequate electrical conductivity, and the need to spend power on artificial ionization severely limits performance of hypersonic MHD devices.<sup>15, 28-30, 36, 37</sup> Indeed, the work done on an electron by the induced Faraday electric field during the electron's lifetime with respect to dissociative recombination with ions is:

$$\varepsilon = e E V_{dr}^e \frac{1}{\beta n_+} = \frac{(eE)^2}{mk_{en} \beta n n_e} = \frac{(ekuB)^2}{mk_{en} \beta n n_e} \quad (6)$$

where  $k$  is the load factor,  $E = kuB$  is the induced electric field,  $V_{dr}^e = \frac{eE}{mk_{en}}$  is the electron drift velocity, and  $\beta$  is the dissociative recombination rate constant. For efficient self-powered operation of the MHD device,  $\varepsilon$  must be substantially larger than the energy cost,  $W_i$ , of a newly produced electron. Specifically, the ratio

### 3 Workshop “Thermochemical processes in plasma aerodynamics”

$$\alpha \equiv \frac{W_i}{\varepsilon} = \frac{mk_{en}\beta n n_e W_i}{(ek_u B)^2} \quad (7)$$

must be limited to a number less than 1. This obviously limits the electron density  $n_e$  and the conductivity, so that the maximum interaction parameter per unit length is:

$$S/L = \frac{\alpha}{\beta W_i} \times \left( \frac{e^2 k M_n}{k_{en} m} \right)^2 \times \frac{B^4}{1 + \frac{M_n e^2 B^2}{mk_{en} k_{n+} \rho^2}} \times \frac{u}{\rho^3} \quad (8)$$

Assuming that the MHD device is located downstream of a single oblique shock with a small turning angle  $\theta$ , we obtain the final expression for the maximum Stuart number per unit length:

$$\frac{S}{L} = \left( \frac{e^2 k M_n}{k_{en} m} \right)^2 \times \frac{\alpha f^4 B^4 u_\infty^7}{8g \beta W_i q^3} \times \left( 1 + \frac{f^2 e^2 M_n B^2 u_\infty^4}{4k_{en} k_{n+} q^2} \right)^{-1} \quad (9)$$

where  $q$  is the flight dynamic pressure, and

$$f(M, \theta) = \frac{\gamma - 1}{\gamma + 1} + \frac{32}{(\gamma + 1) \left[ (\gamma + 1) M \tan \theta + \sqrt{(\gamma + 1)^2 M^2 \tan^2 \theta + 16} \right]^2}$$

$$g(M, \theta) = 1 - \frac{4M \tan \theta}{(\gamma + 1) M \tan \theta + \sqrt{(\gamma + 1)^2 M^2 \tan^2 \theta + 16}}$$

MHD performance as expressed by Eq. (9) is inversely proportional to the energy cost of producing an electron,  $W_i$ . Thus, minimization of  $W_i$  is critical. As shown in our earlier work,<sup>2, 15, 17, 23</sup> electron beams represent the most efficient nonequilibrium method of ionization, with  $W_i = 34$  eV, and in what follows, we will assume that ionization is done by electron beams, with  $W_i = 34$  eV, and that  $\alpha$  is limited to 0.3.

The maximum interaction parameter (9) increases very rapidly with increasing magnetic field and flight speed, and with decreasing dynamic pressure. The very sharp  $u_\infty^7$  dependence is due to both increase in the Faraday e.m.f. with flow velocity and to the decrease in gas density at constant  $q$ . Figure 6 shows  $S/L$  calculated with Eq. (9) versus flight Mach number at 4 different magnetic field strengths and 2 values of flight dynamic pressure. The load factor value was constant at  $k=0.5$ .

Note that in Faraday MHD devices, Hall current is eliminated by segmenting electrodes.<sup>49</sup> However, as the longitudinal Hall electric field increases, arcing between the

### 3 Workshop “Thermochemical processes in plasma aerodynamics”

electrode segments can occur.<sup>49</sup> The arcing would essentially result in a continuous-electrode Faraday device, with dramatic reduction in performance. Denoting the value of Hall field corresponding to the arcing threshold as  $E_c$ , the upper limit for the interaction parameter per unit length becomes with this constraint,

$$\frac{S_{\text{lim}}}{L} = \frac{\alpha g e^2 E_c^2 u_\infty}{2 \beta W_i q} \times \left( 1 + \frac{g e E_c u_\infty}{2(1-k)k_{n+q}} \right)^{-1} \quad (10)$$

This formula does not explicitly depend on  $B$  field and has a weak dependence on flight conditions, because at each flight regime,  $B$  field is adjusted to satisfy the  $E_c$  constraint.

Fig. 6 shows the Hall field-limited interaction parameter of Eq. (10) at two values of  $E_c$ . While the performance is quite good at  $E_c = 50$  kV/m, it is unacceptably low with  $E_c = 5$  kV/m. Therefore, determining the threshold field for intersegment arcing is critical for assessing performance of hypersonic MHD devices.

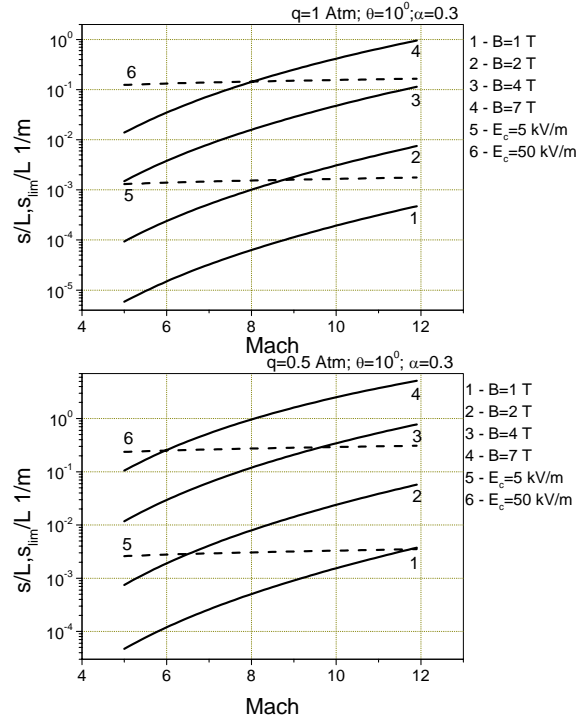


**Fig. 6.** Maximum MHD interaction parameter per unit length versus flight Mach number. Solid lines – interaction parameter at different values of magnetic field, with no constraint on Hall field; dashed lines – upper limit of interaction parameter imposed by constraint on maximum allowed Hall field.

For MHD control of the boundary layer, one can define an MHD interaction parameter with respect to shear stress at the wall:

$$S_\tau = \frac{\sigma B^2 L}{\rho u'} \quad (11)$$

### 3 Workshop “Thermochemical processes in plasma aerodynamics”

where  $u'$  is the friction velocity defined by  $\rho u'^2 = \tau$ , where the wall shear stress can be related to freestream conditions  $\rho$ ,  $u$ , and the friction drag coefficient

$$\tau = \frac{1}{2} \rho u^2 c_f \quad (12)$$

If, for estimates, we assume that the conductivity  $\sigma$  and the density  $\rho$  near the wall are equal to those in the core flow (this can be ensured by wall cooling and by contouring the profiles of ionizing beams), then:

$$S_\tau = \sqrt{\frac{2}{c_f}} \times \frac{\sigma B^2 L}{\rho u} = \sqrt{\frac{2}{c_f}} \times S \quad (13)$$

In the range  $\text{Re}_x^* = 10^5 - 10^7$ , the MHD interaction parameter with respect to wall shear stress greatly exceeds  $S$ :  $S_\tau \approx 30S$ . This may have interesting implications for wall friction and transition control. Of course, MHD effects on the boundary layer can be quite complex. If the load factor  $k$  is not close to 1 or 0, then the heating effects should be comparable to those of ponderomotive  $\vec{j} \times \vec{B}$  forces both in the core flow and near the wall. Also, if the MHD region extends into the core flow, the changes in the core flow would also affect the boundary layer.

#### **4. MHD inlet control at $M > M_{\text{design}}$**

An attractive scenario for MHD inlet control that has been analyzed by several groups,<sup>15-26,28-30,36,37</sup> is to design the vehicle for a relatively low Mach number (for example, Mach 5 or 6), and, at high Mach numbers, move the shocks from inside the inlet back to the cowl lip by an MHD generator device placed at one of the compression ramps. This method, while providing some flexibility of flow control, would not require any net power to run the MHD device, since the generator mode would be used, and the power requirements for air ionization can be minimized with electron beams as ionizers.<sup>15,28-30,36,37</sup> Principal disadvantages of the method include stagnation pressure losses due to the inevitable Joule heating, and also weight of the magnet and other hardware.

In our recent paper,<sup>36</sup> we demonstrated that this approach to MHD inlet control can yield an acceptable inlet performance, while operating in the mode of net power extraction. We showed that the MHD region should be quite short (typically 25-30 cm along the flow) and be located as far upstream as possible.<sup>36</sup> While encouraging, those results relied upon the assumption that the magnetic coil is very large: the coil diameter was assumed to be equal to the forebody width. Minimizing the magnet size by optimizing the MHD region would be important for the practicality of the concept.

### 3 Workshop “Thermochemical processes in plasma aerodynamics”

In this paper, as in Ref. 37, we build upon our earlier work and attempt to optimize the MHD region, so that the magnet size is minimized, while restoring the shock-on-lip condition and operating in the self-powered mode.

#### 4.1. The model

As in Refs. 15, 36, and 37, we consider hypersonic gas flow along a series of compression ramps upstream of the inlet with a forward-shifted cowl lip. The flow is two-dimensional in  $(x, z)$  plane. Cases both without and with MHD influence on the flow were computed. In MHD cases, both magnetic field and ionizing electron beam were directed parallel to  $z$ -axis. Because the entire flow region is hypersonic, steady state solution using  $x$  as marching coordinate can be found.

The set of steady-state Euler equations in Cartesian coordinates, together with an ideal gas equation of state, a simple model of an ideal Faraday MHD generator, vibrational relaxation, and a plasma kinetic model are those of Refs. 15, 36, and 37. Two significant changes were made to the code used in Ref. 36. First, the potentiality of electric field,  $\nabla \times \vec{E} = 0$ , was enforced, which, combined with nonuniformity of flow parameters and magnetic field, results in non-trivial corrections. Indeed, consider a flow at a velocity  $u$  along  $x$  coordinate. The magnetic field is  $B=B_z$ , and the electrical conductivity is  $\sigma$ . In general,  $u = u(x, z)$ ;  $B = B(x, z)$ ;  $\sigma = \sigma(x, z)$ . The width of MHD region along  $y$  will be denoted as  $H$ .

The Faraday current density is:

$$j_y(x, z) = \sigma(x, z)(u(x, z)B(x, z) - E_y) \quad (14)$$

where the electric field  $E_y = \text{const}$ , independent of  $x$  and  $z$ , to satisfy the condition  $\nabla \times \vec{E} = 0$ .

The total current collected on an external resistor  $R$  is:

$$\begin{aligned} I &= \iint_{x,z} j_y(x, z) dx dz \\ &= \iint_{x,z} \sigma(x, z)(u(x, z)B(x, z) - E_y) dx dz \\ &= \iint_{x,z} \sigma u B dx dz - E_y \iint_{x,z} \sigma dx dz \end{aligned} \quad (15)$$

The Ohm's law for the closed circuit can be written as:

$$u(x, z)B(x, z)H = \frac{j_y(x, z)}{\sigma(x, z)}H + IR. \quad (16)$$

Substituting  $j_y(x, z)$  from (14) and  $I$  from (15) into (16), and solving the resulting equation for  $E_y$ , we obtain:

$$E_y = \frac{R \iint_{x,z} \sigma u B dx dz}{H + R \iint_{x,z} \sigma dx dz}. \quad (17)$$

### 3 Workshop “Thermochemical processes in plasma aerodynamics”

The total electrical resistance of the nonuniform plasma region is:

$$r = \frac{H}{\iint_{x,z} \sigma dx dz}, \quad (18)$$

and the load factor is:

$$k \equiv \frac{R}{R+r} = \frac{R}{R + \frac{H}{\iint_{x,z} \sigma dx dz}}. \quad (19)$$

From (19), the external resistance  $R$  can be expressed in terms of the plasma conductivity and the load factor:

$$R = \frac{k}{1-k} H \frac{1}{\iint_{x,z} \sigma dx dz}. \quad (20)$$

Inserting (20) into (17), we obtain the formula for electric field:

$$E_y = \frac{k \iint_{x,z} \sigma u B dx dz}{\iint_{x,z} \sigma dx dz}. \quad (21)$$

This formula is a generalization for non-uniform cases of the familiar expression  $E_y = kuB$  used in the case of uniform flow properties and magnetic fields.

MHD computations start with calculation of the electric field with formula (9). Then, local current density is found from (14). Since the conductivity and velocity profiles in the MHD region can only be determined from the computations, the computational procedure is, by necessity, iterative.

Since the field (21) is essentially an average value of  $uB$ , multiplied by  $k$ , then, according to Eq. (14), in the regions where the local  $uB$  is less than the average value times  $k$ , current will flow in the reverse direction.

External parameters of the MHD circuit, the current  $I$  and the voltage  $V$ , are calculated easily:

$$I = (1-k) \iint_{x,z} \sigma u B dx dz \quad (22)$$

$$V = E_y H = H \frac{k \iint_{x,z} \sigma u B dx dz}{\iint_{x,z} \sigma dx dz} \quad (23)$$

The second modification of the computational procedure relates to modeling of power deposition and ionization by the electron beams. In our earlier work,<sup>15, 28-30, 50-53</sup> we used the so-

### 3 Workshop “Thermochemical processes in plasma aerodynamics”

called ‘forward-backward’ approximation<sup>54</sup> for electron beam propagation along magnetic field lines into gases and beam-generated ionization. More recently, having analyzed the physics of ionization processes and results of experiments and computations, we concluded that in a uniform gas the ionization rate profile is to be close to a truncated Gaussian.<sup>15,36</sup> The simplified model was then developed and used for MHD analyses.<sup>15,36</sup> However, the Gaussian model assumed that the electron beam is monoenergetic at its injection point. If the injected beam electrons have a range of energies, the resulting power deposition and ionization profiles can be obtained as linear superpositions of the Gaussian profiles with appropriate weights. To turn this statement around, any beam power deposition profile can be represented as a linear combination of a finite or infinite number of Gaussian profiles, corresponding to a certain initial energy spectrum of the beam electrons.

Thus, we can, in principle, select a beam power deposition profile that optimizes the MHD performance, which is done in this paper, and only then calculate the required beam energy spectrum at the injection point (this part is left for a separate future study). In fact, our preliminary analysis showed that the best performance of on-ramp MHD flow/shock control devices is reached with a near-uniform beam power deposition profiles in the vertical ( $x$ ) direction. Indeed, if the beam-induced ionization profile peaks close to the ramp surface, then little MHD effect exists far from the surface, resulting in little effect on the bow shock angle and cowl incidence point. If, on the other hand, ionization peaks far from the surface, the effect on the shock is substantial, but since there is little ionization in the region of strong magnetic field (near the surface), the extracted MHD power is reduced and can be insufficient to run the ionizing electron beams. Therefore, in all calculations presented in this paper, we used a uniform profile of electron beam power deposition throughout the MHD region, characterizing the beams with power deposition density,  $Q_b$ , and dimensions of the ionized region along  $x$  and  $z$ .

For performance assessment of the propulsion system with and without MHD control (the detailed assessment is outside the scope of the present work), the following dimensionless parameters were computed at the inlet throat: mass capture ratio  $k_m$ ;  $k_p$ ; total enthalpy ratio  $k_H$ ; static pressure, density, and temperature ratios  $k_p$ ,  $k_\rho$ , and  $k_T$ ; cooled kinetic energy efficiency,  $\eta_{KE,cool}$ ; and the average Mach number  $M$ . The coefficients  $k$  for mass flow rate and static pressures, temperatures, etc., are the ratios of the respective dimensional values at the throat to the freestream values. Note that mass capture  $k_m$  is calculated by referencing the actual mass flow rate at the throat to the mass flow rate through the inlet capture area at zero angle-of-attack. With this definition,  $k_m$  can exceed 1.

### 3 Workshop “Thermochemical processes in plasma aerodynamics”

In most cases, the flow at the inlet throat is quite non-uniform. In this work, we used the so-called stream-thrust averaging commonly accepted in inlet design.<sup>14</sup> This procedure, described in Ref. 14, effectively takes into account losses of total pressure (entropy increase) that would occur in the isolator when the flow is allowed to settle and to become uniform and parallel to the walls.

#### 4.2. MHD control at $M > M_{\text{design}}$ : methodology of computations, computed cases, and results

The two-dimensional four-ramp inlet geometry,<sup>36,37</sup> designed for Mach 5 flight at 2-degree angle-of-attack, had the ramp angles of 2.5, 8.5, 11, and 13 degrees. The location of the cowl lip was chosen so that the first three oblique shocks would together reach the point slightly upstream of the lip (barely missing the lip); the fourth shock was allowed to hit the cowl. The freestream conditions at both design and off-design (Mach 8) Mach numbers studied in this paper correspond to the flight dynamic pressure of 1000 psf (about 0.5 atm). Table 1 lists freestream conditions: altitude  $h$ , and static pressure and temperature,  $p_0$  and  $T_0$ , in all computed cases.

At Mach numbers greater than 5, the shocks would make contact with the cowl, reducing total pressure at the inlet, and potentially causing very high heat transfer rates at the shock impingement point, and possibly flow separation and engine unstart.

To maximize MHD control performance, the magnetic field should be as strong as possible, and it should protrude from the ramp into the flow as far as possible. The field was assumed to be generated by a superconducting coil placed inside the forebody and projecting magnetic field downward. The field strength at the ramp surface was assumed to be 3-5 Tesla. The field outside the coil is a function of the ratio of the distance from the coil end plane and the coil radius. Thus, the protrusion of the B field into the gas increases with the coil diameter. Obviously, to make the magnetic field reasonably uniform in the spanwise ( $y$ ) direction, non-circular magnets are needed. In the present two-dimensional modeling, however, we used the B field strength as a circular-coil function of  $z$ , with the ‘effective’ coil radius  $R$  that should be minimized in the modeling.

Off the centerline, the B field is not only reduced in magnitude, but it also diverges. Therefore, to maximize the ponderomotive forces pushing the flow and shocks upstream, the MHD interaction region should be concentrated near the centerline of the coil.

The ionization of air in the MHD region is created by electron beams injected from the ramp along magnetic field lines. Concentrating electron beam current in a short region near the magnet centerline would avoid the need to have a large area of the vehicle surface covered by

### 3 Workshop “Thermochemical processes in plasma aerodynamics”

fragile windows or differentially pumped ports, which would have been required in cases of long, distributed MHD interaction regions. As the MHD interaction length  $L$  becomes short, the electrical conductivity  $\sigma$  has to be increased in order to keep the interaction parameter (Stuart number) at the same level as that for a long, distributed MHD region. Since the ionization fraction and the conductivity are proportional to the square root of electron beam current density, shortening the MHD region from 2-3 meters down to 10-20 cm requires increasing the beam current density by 2 orders of magnitude, to 50-100 mA/cm<sup>2</sup>. Aerodynamic windows or differentially pumped plasma portholes may be good candidates for electron beam transmission. Such windows or ports can presumably handle very high electron beam currents, even much higher than 100 mA/cm<sup>2</sup>, in contrast to conventional thin foils.

As discussed in Section 4.1, the beam power deposition profile  $Q_b$  was assumed to be uniform in the entire MHD region:  $x_{MHD} \leq x \leq x_{MHD} + \Delta x_{MHD}; \quad |z - z_b(x)| \leq L_b$ .

The goal of optimization studies was to find the values of parameters corresponding to restoration of the design shock wave configuration at minimal magnet radius, with MHD extracted power satisfying the constraint  $P_b \approx \frac{1}{2} P_{MHD}$ . The latter criterion expresses the condition that the MHD device be self-powered, i.e. that the MHD generated power be just enough to generate the ionizing beams, given the approximately 50% efficiency of electron beam generation.

At a given MHD generator position along the forebody and B-field strength at the ramp surface, optimization parameters are: effective radius of the magnet,  $R$ ; e-beam penetration depth,  $L_b$ ; and MHD channel length,  $\Delta x_{MHD}$ .

For the best performance, the MHD interaction region should be placed as far upstream as possible.<sup>36,37</sup> Indeed, the required linear shift of the shock incidence point at the cowl level is caused by a smaller change in shock angle, and, therefore, by a lower MHD interaction parameter, when the MHD region is moved upstream. Additionally, creating the necessary level of ionization at lower gas density (closer to freestream conditions) requires lower current density and power of the ionizing electron beams. The two requirements for the placement of the MHD interaction region (that the interaction region should be as far upstream as possible, and that it should be close to the magnetic coil centerline) define the minimum distance of about one magnet radius of the MHD interaction region from the nose.

Thus, Cases A (A<sub>1</sub>-A<sub>4</sub>), B, and C correspond to MHD region placed on the first ramp, at the minimal distance from the nose. The principal parameters in these and other cases are listed in Table 2. The inlet performance predictions are listed in Table 4. Table 3 contains the principal MHD parameters: the rate of work by  $\vec{j} \times \vec{B}$  forces,  $P_{\vec{j} \times \vec{B}}$ , the extracted power,  $P_{MHD}$ , the gas

### 3 Workshop “Thermochemical processes in plasma aerodynamics”

heating rate,  $P_J$ , the power deposition into vibrational mode of molecules,  $P_V$ , the power of ionizing electron beams,  $P_b$ , the MHD interaction parameter,  $S$ , the enthalpy extraction ratio,  $\eta$ , the total Faraday current,  $I_y$ , and the Faraday voltage,  $U_{el}$ . Due to the two-dimensionality of the problem, all power quantities  $P$  and  $U_{el}$  are expressed per unit length (1 meter) in the spanwise (y) direction. Note that the total rate of work by  $\vec{j} \times \vec{B}$  forces,  $P_{\vec{j} \times \vec{B}}$ , is spent on 1) irreversible Joule heating that consists of gas heating in the narrow sense,  $P_J$ , and the power deposition into vibrational mode of molecules,  $P_V$ , and 2) the generated electric power,  $P_{MHD}$ :  $P_{\vec{j} \times \vec{B}} = P_{MHD} + (P_J + P_V)$ . The ratio between the extracted power and the rate of dissipation is determined by the load factor. At  $k=0.5$ ,  $P_{MHD} = P_J + P_V = 0.5 P_{\vec{j} \times \vec{B}}$ . Note also that  $P_{MHD} = I_y \times U_{el}$ .

To demonstrate advantages of upstream placement of the MHD region, Cases D and E were computed with MHD region shifted downstream. As seen in Table 2, both  $R$  and  $L_b$  have to be increased in these cases compared with those in Cases A<sub>1</sub> and C. Additionally, due to the more intense flow heating and the need to have a larger e-beam ionized region (longer  $L_b$ ), flow spillage and reduction in air mass capture occur in Cases D and E (see Table 4). Also, although Cases D and E yield higher compression ratios  $k_p$  than Cases A<sub>1</sub> and C, the better compression comes at the expense of reduced total pressure and  $\eta_{KE,cool}$ . Note that our numerous calculations with variation of all parameters showed that for the given design and flight conditions, it is impossible to restore the shock-on-lip condition at Mach 8 with MHD region located at  $x > 13$  m, even with a ‘softened’ self-power condition  $P_{MHD} \geq P_b$ .

Cases A<sub>1</sub>, B, and C clearly demonstrate the trade-off between the strength of magnetic field and the size of the magnet. Comparison of these three cases shows that the magnet size can be reduced and the shock-on-lip condition restored, if the strength of magnetic field is increased (Table 2). However, as seen in Table 4, Case A<sub>1</sub> is the best among these three cases in terms of compression ratio  $k_p$ , kinetic energy efficiency  $\eta_{KE,cool}$ , and enthalpy ratio  $k_H$ . Thus, larger magnets with relatively modest B field strength do work better than smaller magnets with stronger B.

All cases except A<sub>2</sub> had load factors  $k=0.5$ . Case A<sub>2</sub> was run at a higher load factor,  $k=0.75$ . As seen in Table 2, increasing load factor requires larger magnets and longer MHD regions. Calculations at  $k$  less than 0.5, not listed in the tables, showed that the performance becomes worse than that at  $k=0.5$ , because with less power extraction it is difficult to restore the design shock configuration, while demanding that  $P_b \approx \frac{1}{2} P_{MHD}$ . Thus, for optimal performance, the load factor should not deviate far from 0.5.

### 3 Workshop “Thermochemical processes in plasma aerodynamics”

Comparison of Cases A<sub>1</sub>, A<sub>3</sub>, and A<sub>4</sub> demonstrates the role of the magnitude of  $Q_b$  (electron beam power deposition density). As seen in Table 2, at the given flight conditions, the value  $Q_b = 10 \text{ MW/m}^3$  (Case A<sub>1</sub>) is close enough to the optimum for the MHD region to be short,  $\Delta x_{MHD} \leq 0.3 \text{ m}$ , while satisfying the criterion  $P_{MHD} \approx \frac{1}{2} P_b$ . At  $Q_b = 2 \text{ MW/m}^3$  (case A<sub>3</sub>), shock-on-lip condition can be achieved at substantially increased  $R$ ,  $L_b$ , and  $\Delta x_{MHD}$ . At  $Q_b = 50 \text{ MW/m}^3$  (case A<sub>4</sub>), the values of  $R$ ,  $L_b$  and  $\Delta x_{MHD}$  can be decreased as compared with those in the Case A<sub>1</sub>, but only if the criterion  $P_{MHD} \approx \frac{1}{2} P_b$  is relaxed to  $P_{MHD} \approx P_b$ .

Figures 7 and 8 show the location of the MHD region, contour lines of gas and vibrational temperature, and flow streamlines in Cases A<sub>1</sub> and D. As seen in the figures, due to vibrational excitation by electron impact in the MHD region and relatively slow vibrational relaxation in the cold, low-density, weakly dissociated flow, there is a considerable vibrational nonequilibrium at the inlet throat. One challenge posed by this nonequilibrium is that the stream-thrust averaging procedure<sup>14</sup> was developed for thermally equilibrium flows. Fortunately, the kinetic energy efficiency  $\eta_{KE,cool}$  was found to be not very sensitive to the nonequilibrium conditions. Nevertheless, the procedure of stream- thrust averaging should be generalized for nonequilibrium flow in the future.

We assumed the MHD region to be an ideal Faraday generator. The latter assumption is non-trivial. The Hall parameters in the computed cases can reach as high as 10. In conventional Faraday channels with continuous electrodes, MHD effects are sharply reduced due to the Hall effect, while in Faraday channels with segmented electrodes there is a danger of arcing between the electrode segments at high Hall parameters.<sup>49</sup> However, the MHD devices analyzed in this work are very different from conventional devices. Not only is the conductivity non-thermal, generated and controlled by externally injected electron beams, but also the length of the channel (15-30 cm) is much shorter than its width (5 meters). Considering short MHD channel as a “slice” of a long channel, with only 1 electrode segment, one might argue that the performance of such a short channel should be close to that of an ideal Faraday device, even at high Hall parameters. This argument requires an investigation and validation.

Overall, MHD control of hypersonic flows appears promising. Note that the first experimental demonstration of cold-air supersonic MHD effect with non-self-sustained ionization (by repetitive high-voltage nanosecond pulses) has been recently performed at Princeton University.<sup>55</sup>

Table 1. Freestream conditions in computed cases. Freestream dynamic pressure is  $q=1000$  psf.

Mach number	h, km	$p_0$ , Pa	$T_0$ , K
5	24.538	2735	221.09
8	30.76	1068.75	227.26

Table 2. MHD generator cases

Cas e	$Q_b$ , MW/m <sup>3</sup>	$B_0$ , T	R, m	$L_b$ , m	$x_{MHD}$ , m	$\Delta x_{MHD}$ , m	k
A <sub>1</sub>	10	3	1.65	1.65	2	0.3	0.5
A <sub>2</sub>	10	3	1.75	1.65	2	0.375	0.75
A <sub>3</sub>	2	3	2	2.3	2	0.65	0.5
A <sub>4</sub>	50	3	1.3	1	2	0.15	0.5
B	10	4	1.15	1.5	1.25	0.25	0.5
C	10	5	0.8	1.25	1	0.25	0.5
D	10	3	2.6	2.5	9	0.25	0.5
E	10	5	1.5	2.25	9	0.25	0.5

Table3.Computed MHD parameters.

Case	$P_{j \times \vec{B}}$ MW/m	$P_{MHD}$ M W/m	$P_j$ , MW/m	$P_v$ , MW/m	$P_b$ , MW/m	$S$	$\eta$	$I_y$ , kA	$U_{el}$ , kV/m
A <sub>1</sub>	25.4	10	9.21	6.218	4.926	0.12	0.02	6.66	1.5
A <sub>2</sub>	22.8	11.91	7.53	3.41	6.14	0.19	0.024	5.146	2.315
A <sub>3</sub>	32.6	11.89	1.19	8.78	2.97	0.1	0.024	8.67	1.37
A <sub>4</sub>	7.36	7.94	6.62	3.68	7.35	0.15	0.016	4.6	1.72
B	23.33	7.82	8.33	7.17	3.72	0.19	0.016	5.23	1.49
C	20.83	6.07	7.74	7.014	3.098	0.12	0.012	4.27	1.42
D	36.71	14.88	15.03	6.8	7.47	0.1	0.03	9.52	1.56
E	46.1	14.03	18.29	13.76	6.72	0.12	0.28	9.0	1.55

Table 4. Computed inlet parameters with and without MHD control for Mach 5 design. Angle of attack is  $2^\circ$ ; flight dynamic pressure is  $q=1000$  psf for all MHD cases.

Freestream Mach No. and MHD conditions		$k_m$	$k_p$	$k_\rho$	$k_T$	$M$	$\eta_{KE,cool}$	$k_H$
M=5; design, no MHD		1.14	16.07	6.94	2.31	2.822	0.991	1
8	No MHD	1.13	22.01	6.547	3.36	3.94	0.969	1
	A <sub>1</sub>	1.14	22.46	6.8	3.3	3.87	0.924	0.955
	A <sub>2</sub>	1.14	21.92	6.78	3.23	3.92	0.926	0.956
	A <sub>3</sub>	1.13	23.09	6.83	3.37	3.78	0.911	0.945
	4							
	A <sub>4</sub>	1.14	23.18	6.75	3.43	3.82	0.943	0.976
	B	1.14	20.39	6.773	3.01	4.07	0.919	0.944
	C	1.14	19.66	6.74	2.91	4.16	0.92	0.943
	D	1.09	30.41	6.85	4.43	3.16	0.91	0.966
	E	1.11	35.62	7.26	4.9	2.89	0.886	0.95

#### 4.3. The effect of current reversal

As discussed in Section 4.1, in those areas within the MHD region where the local value of  $uB$  is less than the average value multiplied by  $k$ , the electric current should flow in the direction opposite to the Faraday electromotive force. This effect was indeed observed in all computed cases. As an example, Fig. 9 shows the current profile in Case E. As seen in the Figure, the current density reduces to zero far from the ramp, and then becomes negative. In the region of ‘negative’ current, the  $\vec{j} \times \vec{B}$  force reverses direction and becomes an accelerating force. Although the effect was seen in all computed cases, the results were not changed much by it. However, it is conceivable that in some other MHD problems the current reversal can play a significant role.

Consider, for example, the near-wall region of an MHD generator. If the  $B$  field is normal to the surface, and the conductivity is more or less uniform across the boundary layer, then close enough to the wall, where the velocity is less than the freestream

velocity multiplied by the load factor, the  $\vec{j} \times \vec{B}$  will accelerate the boundary layer. This effect can, in principle, change the boundary layer structure and thickness, and can affect vorticity generation, flow separation, and laminar-turbulent transition. These phenomena should be investigated in future.

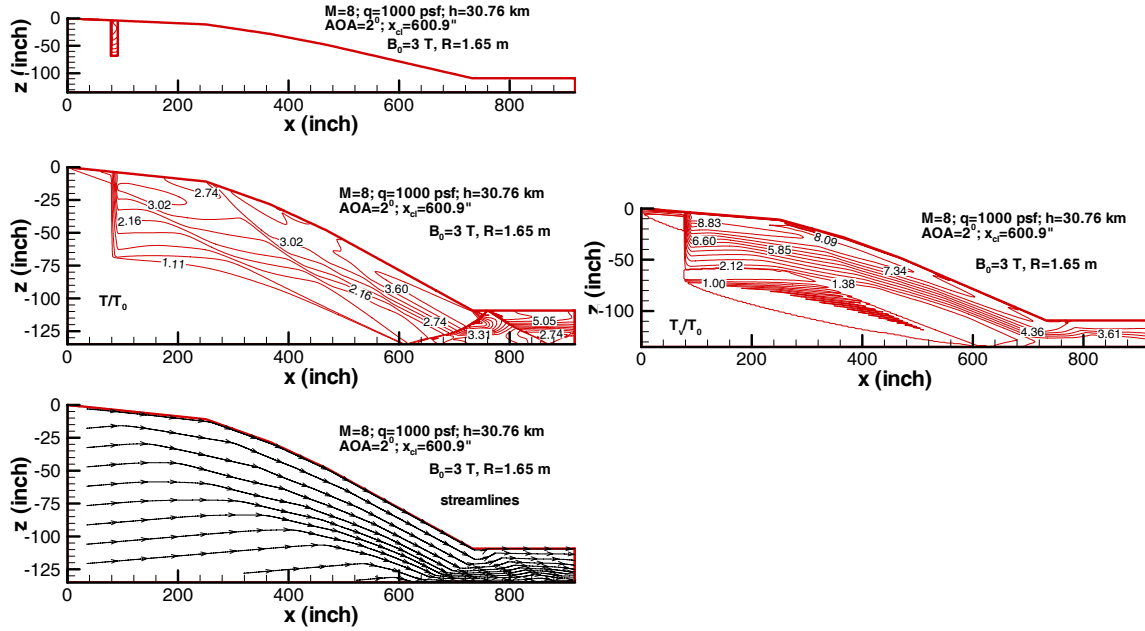


**Fig. 7.** Location of the MHD interaction region, contours of gas and vibrational temperatures, and streamlines at Mach 8 with MHD control for the case of magnet with  $B_0=3$  T;  $R=1.65$  m (Case A<sub>1</sub>)

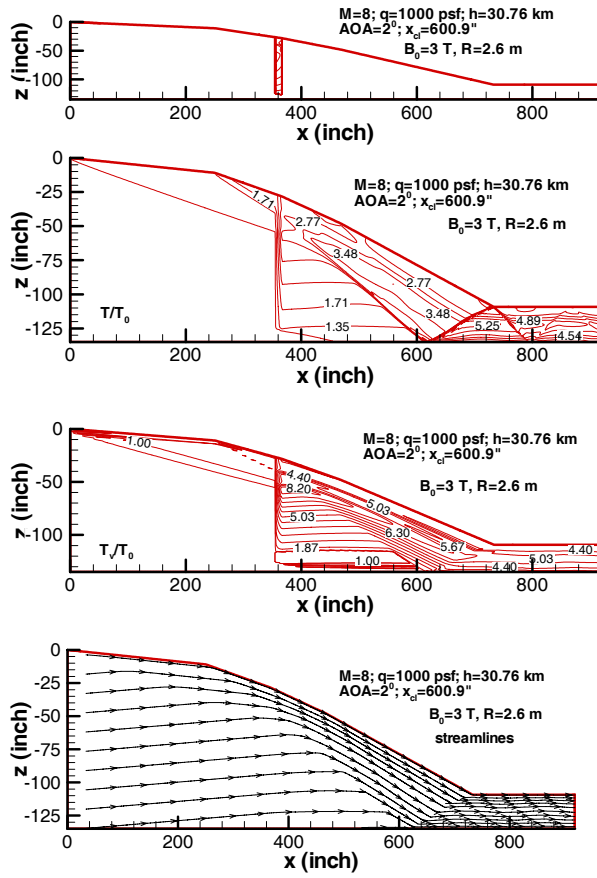


**Fig. 8.** Location of the MHD interaction region, contours of gas and vibrational temperatures, and streamlines at Mach 8 with MHD control for the case of magnet with  $B_0=3$  T;  $R=2.6$  m (Case D)

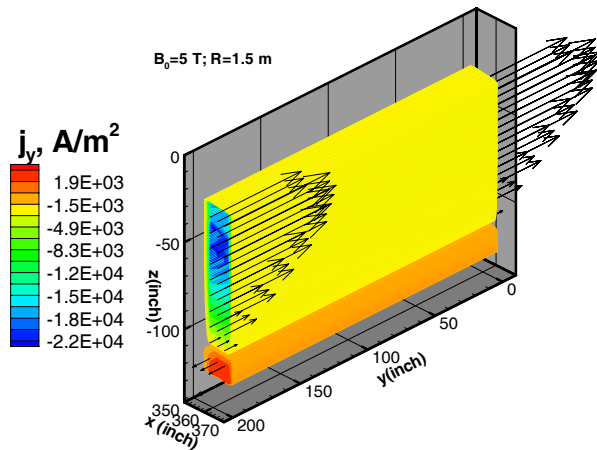


**Fig. 9.** Current density profile and directions in the MHD region for Case E.

## 5. Air capture increase with Virtual Cowl

The Virtual Cowl concept<sup>15, 35</sup> is schematically shown in Fig. 10. We considered 2D hypersonic gas flow along a series of compression ramps upstream of the inlet; cases both without and with heat addition were computed with the set of Euler equations together with perfect gas equation of state. Because the entire flow region is supersonic, a steady state solution using  $x$  as marching coordinate can be found. The heat addition rate profile was set as Gaussian, that is, it was proportional to  $\exp\left(-\left(x-x_0\right)^2/r_{eff,x}^2 - \left(z-z_0\right)^2/r_{eff,z}^2\right)$ , where  $x_0$  and  $z_0$  are coordinates of the center of the heating region, and  $r_{eff,x}$  and  $r_{eff,z}$  are the effective radii. The parameters  $x_0$ ,  $z_0$ ,  $r_{eff,x}$ , and  $r_{eff,z}$  were varied in computations in order to find optimal values of these parameters. In “circular-cylinder Gaussian” cases,  $r_{eff,x} = r_{eff,z} = r_{eff}$ . In “elliptical-cylinder Gaussian” cases,  $r_{eff,x} \neq r_{eff,z}$ , the heating profile may also be tilted at an angle  $\alpha_q$  with respect to  $x$  axis.

The inlet performance was characterized by the set of stream-thrust averaged parameters, as in the MHD control studies in Section 4.

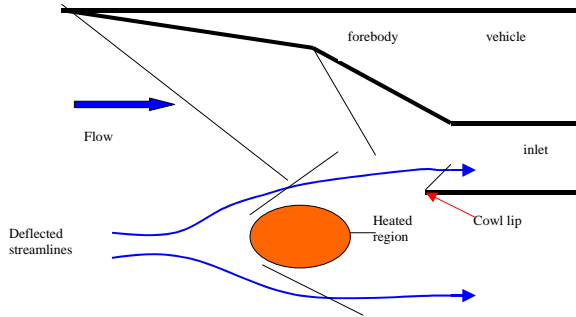


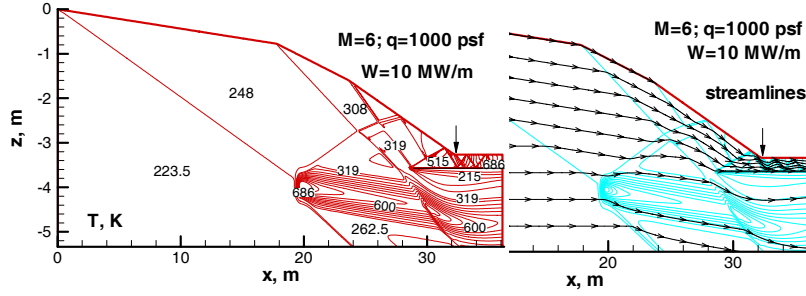
**Fig. 10.** Schematic diagram of the virtual cowl concept: off-body heat addition increases mass capture.

Freestream conditions in computed cases corresponded to flight at Mach 6, 8, or 10, with dynamic pressure of either 1000 psf or 2000 psf. The baseline case was that of Mach 10 flight with zero-degree angle-of-attack. The 3-ramp inlet ( $2.5^\circ$ ,  $8.0^\circ$ , and  $11.0^\circ$  ramp angles) was chosen so that the nose shock would barely (by about 1 inch) miss the cowl lip, and the flow would be almost parallel to the isolator walls downstream of the inlet throat.

To reduce the spillage, the cowl might be extended upstream, although this could be difficult to accomplish practically. However, the case with extended solid cowl can serve as a guide to optimizing virtual cowl cases. Qualitatively, one would expect that the virtual cowl (i.e., off-body energy addition) should, for the best performance, create a flow pattern imitating that of the solid extended cowl. Since shocks do not reflect off a heated region, the analogy between the solid and virtual cowls is not exact. However, the heated region can generate a shock wave that would mimic the shock reflected from the solid surface upon incidence of the nose shock on it. Thus, one would expect that the energy addition should be more or less concentrated, and that it should be positioned near the intersection of the nose shock with the upstream continuation of the cowl.

Note that heating and the resulting expansion of the gas would adversely affect both mass flow rate and stagnation pressure at the throat if the heated air is allowed to enter the inlet. Therefore, the energy addition region should be shifted somewhat down, so that heated and expanded air would miss the inlet, while cold air would be compressed and deflected into the inlet.

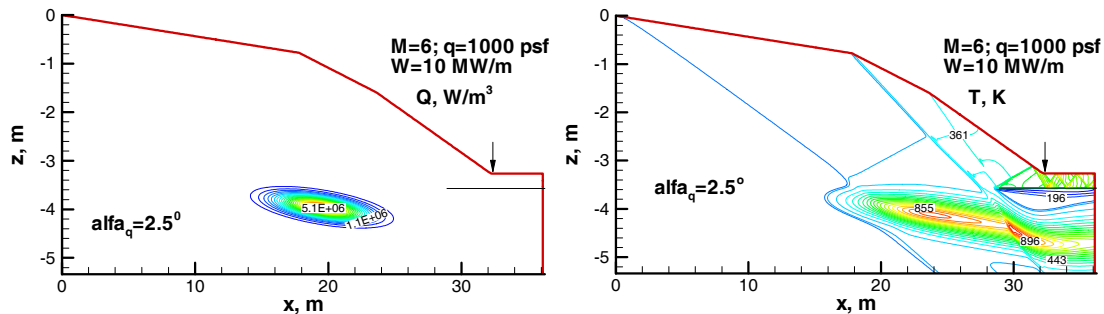
The qualitative expectations of the preceding two paragraphs were confirmed in calculations.<sup>35</sup> With “circular-cylinder Gaussian” heat addition,  $r_{eff,x} = r_{eff,z} = r_{eff} = 0.2 \text{ m}$  was found to be close to the optimum. Calculations showed that energy addition does increase the mass capture, and the effect becomes stronger as more energy is added. With varying coordinate of the heated region, the mass capture and the enthalpy flux both exhibit broad maxima at the value of  $x$  approximately corresponding to the intersection of the nose shock with the upstream continuation of the cowl. Total pressure and adiabatic kinetic energy coefficients also have their peaks, but at a value of  $x$  somewhat shifted downstream with respect to that where mass capture is maximum. As predicted in the previous paragraph, shifting the center of energy addition region by  $2r_{eff} = 0.4 \text{ m}$  down from the cowl line somewhat improves inlet performance. Static temperature contours and flow streamlines in Mach 6, 1000 psf case with energy addition rate of  $W=10 \text{ MW/m}$  centered near the optimum location are shown in Fig. 11.



**Fig. 11.** Static temperature contour lines (upper plot) and flow streamlines (lower plot) at Mach 6, 1000 psf, with optimum location of “circular Gaussian” Virtual Cowl with  $r_{eff} = 0.2 \text{ m}$ ,  $W=10 \text{ MW/m}$ .

We found that if, instead of a single energy addition region, two energy addition regions are used with the total power equal to that of the single region, then, with proper positioning of the second source downstream of the first one, the inlet performance would not decrease compared with that given by the single source.<sup>35</sup>

We have also run a series of calculations with “elliptical-cylinder Gaussian” heating profiles,  $r_{eff,x} \neq r_{eff,z}$ . Stretching the energy addition profile along the flow, while maintaining constant total power, was found to result in a small improvement in inlet performance. Specifically,  $r_{eff,x} = 15r_{eff,z}$  was found to give the best performance. We further found that slightly tilting the stretched heating profile with respect to  $x$  axis can improve the performance. The optimum angle turned out to be  $\alpha_q = 2.5^\circ$ , which, perhaps not coincidentally, equals the angle of the first ramp. Fig. 12 illustrates the optimum case with stretched and tilted heating profile at Mach 6. Overall, although stretched and tilted heating profiles do perform better than the “circular” ones, the improvement is only incremental.<sup>35</sup>



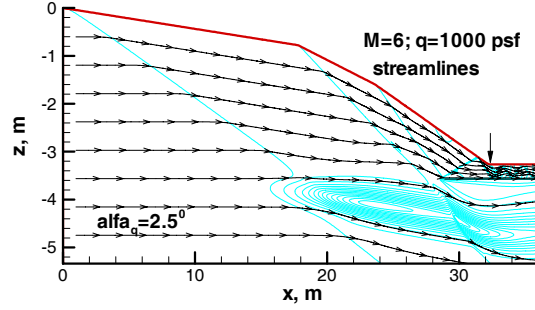


**Fig. 12.** Upper plot: power density of the optimally located, stretched, and tilted 10 MW/m source. Middle and lower plot: static temperature contours and flow streamlines at Mach 6, 1000 psf, with that heating source.

Finally, the constraint that the energy addition has to be placed at or only slightly below the cowl level was relaxed.<sup>35</sup> For the Mach 6, 1000 psf flight, the “circular-cylinder Gaussian” heating profile with  $r_{eff} = 0.2$  m and the total power of 5 MW/m was positioned at different vertical locations  $z$  below the cowl level  $z_{cl}$ . The streamwise coordinate of the center of energy addition region was held constant at  $x_Q = 0.5, 5.5,$  and  $10.5$  m. In each case, the best inlet performance turned out to occur when the shock generated by the energy addition passed through the point of intersection of the nose shock with the upstream continuation of the cowl line, as expected. The best  $\eta_{KE}$  achieved was equal, and the best  $k_m$  only incrementally superior to those in the case with energy addition slightly below the cowl level. Given that the performance increase is small, and that it can be practically difficult to implement and control energy addition far from the vehicle surface, it appears advantageous to work with energy addition at or slightly below the cowl level. It is instructive, however, to note that, although matching the  $k_m$  given by the extended solid cowl at Mach 6 does not seem possible with energy addition concentrated at or just below the cowl line, increasing the power of the heating source while moving the source away from the body can yield the  $k_m$  equal to that of the solid cowl. Indeed, having run cases with power depositions of 20 and 35 MW/m, we found that the 35 MW/m case does match the  $k_m$  of extended solid cowl, although with somewhat lower  $\eta_{KE}$ . Note that at power levels as high as 35 MW/m, the optimum

location of the energy addition should be farther from the body; this was not fully computed in the present work.

The energy required for the Virtual Cowl may be supplied by an in-stream MHD power extraction system, in which case the additional mass flow may come at the expense of enthalpy taken from the propulsive flowpath. In this work, sample scramjet engine cycles were used to assess the impact of additional captured flow and enthalpy extraction.

The following six cases were analyzed. Cases A and B represent two Mach 8 conditions with two levels of optimized “circular Gaussian” energy deposition, 5 MW/m and 10 MW/m, respectively. Cases C to F represent Mach 6 conditions at different energy deposition levels and locations: Case C corresponds to the optimized “circular Gaussian” energy deposition of 5 MW/m; Case D corresponds to the optimized “circular Gaussian” energy deposition of 10 MW/m; Case E corresponds to the optimized “tilted elliptical Gaussian” ( $r_{eff,x} = 3$  m,  $r_{eff,z} = 0.2$  m,  $\alpha_q = 2.5^\circ$ ) energy deposition of 10 MW/m; and Case F corresponds to the “circular Gaussian” energy deposition of 35 MW/m located far from the cowl lip ( $x_Q = 18.5$  m,  $z_{CL} - z_Q = 1.3$  m). The results of the inlet calculations are shown in third through fifth columns of Table 5. The results show that for energy extractions on the order of 1.2% to 3.4%, the mass flow through the engine can be increased by 7.1% to 15.5% with little change in the inlet efficiency.

Sample engine calculations were conducted at Mach 6 and 8 for a baseline Mach 10 design operating on hydrogen fuel. The baseline engine calculations assumed  $\eta_{KE} = 0.97$ , combustion efficiency = 0.9, and nozzle efficiency = 0.97. The assumed inlet kinetic energy efficiency ( $\eta_{KE} = 0.97$ ) was chosen to represent typical values for an inlet including friction effects. The inlet efficiency results from the Virtual Cowl analysis were applied as a delta to the assumed 0.97 value.

The effects of the virtual cowl on the engine performance were assessed by increasing the mass flow, modifying the inlet kinetic energy efficiency, and removing the required enthalpy from the scramjet combustor. Note that this analysis assumes that the energy deposited to create the virtual cowl is obtained from the scramjet combustor and the efficiency of the energy extraction is 100%.

The results of the engine cycle calculations are shown in the last two columns of Table 5, where it can be seen that the engine thrust coefficient  $C_T$  increases nearly proportionally to the mass flow increase. The effect of the virtual cowl on the engine specific impulse is seen to be relatively small (i.e. less than 1%). Thus, the virtual cowl appears to represent a system for augmenting the thrust of a scramjet engine with little impact on overall cycle efficiency. (Apparently, the additional compression achieved with the additional captured mass flow offsets the enthalpy extraction from the combustor.)

The results from the engine cycle calculations show that the application of a virtual cowl merits additional investigation. While the required energy deposition levels are high (5-35 MW per meter of engine width), and the weight impacts of power extraction and energy deposition systems have not been estimated, the ability to increase the engine thrust of an engine for an accelerating system can be significant.

Two additional sets of engine cycle calculations were conducted to further assess the impact of the virtual cowl concept. In the first set of calculations, the effects of the virtual inlet were included in the calculation, but no energy was extracted from the propulsion flowpath. This set of calculations applies in the case when the energy needed for production of the virtual cowl is either carried inside the vehicle or produced with an on-board system that does not impact the engine. In the second set of calculations, the virtual cowl was not used, but the energy that would be needed was assumed to be applied to the combustor. This set of calculations was conducted as a reference and would correspond to the case when the additional energy is available (either carried on-board or produced separately from the propulsive flowpath) and supplied directly to the combustor.

The results from the two sets of engine calculations are compared to the virtual cowl results in Table 6. The results show that the engine performance is better for the virtual cowl when the energy is not extracted from the flowpath. This is the expected result since energy extraction is equivalent to a reduction in fuel supplied to the combustor. The last set of calculations shows the impact of energy deposition within the combustor. In this case, the calculations assume that the energy is available on-board and directly deposited in the combustor. The results show that both the thrust coefficient and

specific impulse increase by small percentages. These results show that the principal advantage of the virtual cowl is the increase in engine thrust (primarily caused by the increase in captured airflow) with little change in specific impulse regardless of where the energy for production of the virtual cowl is obtained.

Table 5. Virtual Cowl impact on engine performance

Case	Freestream Mach Number	Enthalpy Extracted	Mass Flow Increase	$\Delta\eta_{KE}$	$\Delta C_T$	$\Delta I_{sp}$
A	8	1.2%	7.1%	+0.002	+6.8%	-0.27%
B	8	2.3%	11.4%	+0.002	+10.5%	-0.82%
C	6	1.8%	7.8%	+0.004	+8.0%	+0.20%
D	6	3.4%	13.9%	0.0	+14.0%	+0.05%
E	6	3.4%	15.5%	+0.003	+15.8%	+0.27%
F	6	10.2%	34.5%	-0.003	+33.6%	-0.52%

Table 6. Comparison of virtual cowl with and without energy extraction, and effect of energy deposition in combustor.

		Virtual Cowl with Energy Extraction		Virtual Cowl without Energy Extraction		No Virtual Cowl and Energy Addition	
Case	Freestream Mach Number	$\Delta C_T$	$\Delta I_{sp}$	$\Delta C_T$	$\Delta I_{sp}$	$\Delta C_T$	$\Delta I_{sp}$
A	8	+6.8%	-0.27%	+7.6%	+0.46%	+0.78%	+0.78%
B	8	+10.5%	-0.82%	+12.0%	+0.57%	+1.48%	+1.48%
C	6	+8.0%	+0.20%	+8.7%	+0.78%	+0.63%	+0.63%
D	6	+14.0%	+0.05%	+15.1%	+1.10%	+1.18%	+1.18%
E	6	+15.8%	+0.27%	+17.0%	+1.30%	+1.18%	+1.18%
F	6	+33.6%	-0.52%	+37.2%	+2.17%	+3.50%	+3.50%

### **Acknowledgements**

The work was supported by the Air Force Office of Scientific Research, DARPA, Air Force Research Laboratory, and by Boeing Phantom Works (St. Louis, Missouri). The authors express their gratitude to Philip Smereczniak and Joseph Silkey of Boeing Phantom Works, and to Ramon Chase of ANSER Corp. for their support and valuable discussions and advice.

### **References**

1. Oswatich, K., "Propulsion with Heating at Supersonic Speed," Report 90, Deutsche Versuchsanstalt fuer Luft und Raumfahrt, 1959.
2. "The Flow of Gas with a Supply of Heat Near the Outer Surface of a Body," Survey, Byur. Nauchn. Techn. Inform., Tsentral. Aero-Gidrodinam.Inst., No.347 (1971) (in Russian)
3. "Study of Flows with a Heat Supply Near the Outer Surface of an Aircraft," Survey, Byur. Nauchn. Techn. Inform., Tsentral. Aero-Gidrodinam.Inst., No.617 (1982) (in Russian)
4. Georgievskii, P.Yu., and Levin, V.A., "Supersonic Flow Past Volume Sources of Energy Release," in: Mekhanika. Sovremennye problemy (Mechanics: Modern problems) Moscow: MGU, 1987, p.93 (in Russian)
5. Levin, V.A., and Terent'eva, L.V., "Supersonic Flow Over a Cone with Heat Release in the Neighborhood of the Apex," Izv. RAN, MGG, 1993, No. 2, p. 110-114 (in Russian)
6. Georgievskii, P.Yu., and Levin, V.A., "Supersound Body Bypass with External Resources of Heat Release," Pis'ma Zhurn.Tekhn. Fiz., 1988, Vol.14, No. 8, pp. 684-687 (in Russian)
7. Georgievskii, P.Yu., and Levin, V.A., "Nonstationary Interaction of Sphere with Atmospheric Temperature Heterogeneities in Supersonic Flow," Khimicheskaya Fizika, 1993, V. 10, No. 12, pp. 1414-1423 (in Russian)
8. Borzov, V.Yu., Ribka, I.V., and Yuriev, A.S., "The Influence of Local Energy Supply at Hypersonic Flow on Wave Drag of Bodies of Different Blunting," Inzh. Fiz. Zh., 1992, Vol. 63, No. 6, pp. 659-664 (in Russian)

9. Belotserkovskii, O.M., Grudnitskii, V.G., and Prokhorchuk, Yu.A., "Difference Scheme of 2<sup>nd</sup> Order of Accuracy on the Minimal Pattern for Hyperbolic Equations," USSR Comp. Math. Math. Phys., 1983, Vol. 23, No. 1, pp. 81-86 (in Russian)
10. Riggins, D., Nelson, H.F., and Johnson, E., "Blunt-Body Wave Drag Reduction Using Focused Energy Deposition," AIAA J., 1999, Vol. 37, No. 4, pp. 460-467.
11. Knight, D., Kuchinskiy, V., Kuranov, A., and Sheikin, E., "Aerodynamic Flow Control at High Speed Using Energy Deposition," 4<sup>th</sup> Int. Workshop on Magneto-Plasma Aerodynamics for Aerospace Applications, Moscow, 2002.
12. Knight, D., Kuchinskiy, V., Kuranov, A., and Sheikin, E., "Survey of Aerodynamic Flow Control at High Speed by Energy Deposition," AIAA Paper 2003-0525.
13. Shneider, M.N., Macheret, S.O., Zaidi, S.H., Girgis, I., Raizer, Yu.P., and Miles, R.B., "Steady and Unsteady Supersonic Flow Control with Energy Addition," AIAA Paper 2003-3862, 34<sup>th</sup> AIAA Plasmadynamics and Lasers Conference, Orlando, FL, 23-26 June 2003.
14. Van Wie, D.M., "Scramjet Inlets," in: Scramjet Propulsion, Edited by E.T. Curran and S.N.B. Murthy, Progress in Astronautics and Aeronautics, Vol. 189, American Institute of Aeronautics and Astronautics, Inc., Reston, VA, 2000, Chapter 7, pp. 447-511.
15. Shneider M.N., Macheret S.O., and Miles R.B., "Nonequilibrium Magnetohydrodynamic Control of Scramjet Inlets," AIAA Paper 2002-2251, 33<sup>rd</sup> AIAA Plasmadynamics and Lasers Conference, 20-23 May 2002, Maui, Hawaii.
16. Kuranov A.L., and Sheikin, E.G., "MHD Control on Hypersonic Aircraft under AJAX Concept: Possibilities of MHD Generator," AIAA Paper 2002-0490, 2002.
17. Kopchenov V., Vatazhin A., and Gouskov O., "Estimation of Possibility of Use of MHD Control in Scramjet," AIAA Paper 99-4971, 1999.
18. Brichkin D.I., Kuranov A.L., and Sheikin E.G., "The Potentialities of MHD Control for Improving Scramjet Performance," AIAA Paper 99-4969, 1999.
19. Brichkin D.I., Kuranov A.L., and Sheikin E.G., "MHD Technology for Scramjet Control," AIAA Paper 98-1642, 1998.
20. Kuranov A.L. and Sheikin E.G., "The Potential of MHD Control for Improving Scramjet Performance," AIAA Paper 99-3535, 1999.

21. Kuranov, A.L., and Sheikin, E.G., "MHD Control on Hypersonic Aircraft under AJAX Concept: Possibilities of MHD Generator," AIAA Paper 2002-0490, 2002.
22. Golovachev, Yu.P., and Sushikh, S.Yu., "Supersonic Air-Scoop Flows of a Weakly Ionized Gas in External Electromagnetic Field," *Technical Physics*, Vol. 45, No. 2, 2000, p.168.
23. Golovachev, Yu.P., Sushikh, S.Yu., and Van Wie, D., "Numerical Simulation of MGD Flows in Supersonic Media," AIAA Paper 2000-2666, 2000.
24. Vatazhin A., Kopchenov V., and Gouskov O., "Some Estimations of Possibility to Use the MHD Control for Hypersonic Flow Deceleration," AIAA Paper 99-4972, 1999.
25. Kopchenov V., Vatazhin A., and Gouskov O., "Estimation of Possibility of Use of MHD Control in Scramjet," AIAA Paper 99-4971, 1999.
26. Vatazhin A., Kopchenov V., and Gouskov O., "Numerical Investigation of Hypersonic Inlets Control by Magnetic Field," *The 2<sup>nd</sup> Workshop on Magneto- and Plasma Aerodynamics in Aerospace Applications*, Moscow, 5-7 April 2000, pp. 56-63.
27. Bityurin V.A., Klimov A.I., Leonov S.B., Bocharov A.N., and Lineberry J.T., "Assessment of a Concept of Advanced Flow/Flight Control for Hypersonic Flights in Atmosphere," AIAA Paper 99-4820, 1999.
28. Macheret S. O., Shneider M. N., and Miles R. B., "Magnetohydrodynamic Control of Hypersonic Flow and Scramjet Inlets Using Electron Beam Ionization," *AIAA Journal*, Vol. 40, No. 1, 2002, pp. 74-81.
29. Macheret S. O., Shneider M. N., and Miles R. B., "Magnetohydrodynamic and Electrohydrodynamic Control of Hypersonic Flows of Weakly Ionized Plasmas," AIAA Paper 2002-2249, 33<sup>rd</sup> AIAA Plasmadynamics and Lasers Conference, 20-23 May 2002, Maui, Hawaii.
30. Macheret S. O., Ionikh Y. Z., Martinelli L., Barker P. F., and Miles R. B., "External Control of Plasmas for High-Speed Aerodynamics," AIAA Paper 99-4853, 1999.
31. Leonov S., Bityurin V., Savelkin K., and Yarantsev D., "Effect of Electrical Discharge in Separation Processes and Shock Position in Supersonic Airflow," AIAA

- Paper 2002-0355, 40<sup>th</sup> AIAA Aerospace Sciences Meeting and Exhibit, Reno, NV, 13-17 January 2002.
32. Leonov S., Bityurin V., Savelkin K., and Yarantsev D., "The Features of Electro-Discharge Plasma Control in High-Speed Gas Flows," AIAA Paper 2002-2180, 33<sup>rd</sup> AIAA Plasmadynamics and Lasers Conference, 20-23 May 2002, Maui, Hawaii.
  33. Leonov S., Bityurin V., Savelkin K., and Yarantsev D., "Progress in Investigation for Plasma Control of Duct-Driven Flows," AIAA Paper 2003-0699, 41<sup>st</sup> AIAA Aerospace Sciences Meeting and Exhibit, Reno, NV, 6-9 January 2003.
  34. Leonov S., Bityurin V., Youriev A., Savishchenko N., Pirogov S., and Ryzhov E., "Problems in Energetic Method in Drag Reduction and Flow/Flight Control," AIAA Paper 2003-0035, 41<sup>st</sup> AIAA Aerospace Sciences Meeting and Exhibit, Reno, NV, 6-9 January 2003.
  35. Macheret S. O., Shneider M. N., and Miles R. B., "Scramjet Inlet Control by Off-Body Energy Addition: a Virtual Cowl," AIAA Paper 2003-0032, 41<sup>st</sup> AIAA Aerospace Sciences Meeting and Exhibit, Reno, NV, 6-9 January 2003.
  36. M. N. Shneider, S. O. Macheret, and R. B. Miles, "Comparative Analysis of MHD and Plasma Methods of Scramjet Inlet Control," AIAA Paper 2003-0170, 41<sup>st</sup> AIAA Aerospace Sciences Meeting and Exhibit, Reno, NV, 6-9 January 2003.
  37. Macheret S. O., Shneider M. N., and Miles R. B., "Optimum Performance of Electron Beam Driven MHD Generators for Scramjet Inlet Control," AIAA Paper 2003-3763, 34<sup>th</sup> AIAA Plasmadynamics and Lasers Conference, Orlando, FL, 23-26 June 2003.
  38. Seebass R., "Sonic Boom Theory," *Journal of Aircraft*, Vol. 6, No. 3, pp. 177-184, 1969.
  39. McLean F.E., "Configuration design for specific pressure signature characteristics," in: *Sonic Boom Research*, ed. I.R. Schwartz, SP-180, NASA, 1968, pp. 37-40.
  40. Cheng, Sin-I, Patent US 3737119, filed Jun 15, 1970, issued June 5, 1973.
  41. Crow S.C., and Bergmeier G.G., *J. Fluid Mech.*, Vol. 325, 1996.
  42. Miles R.B., Martinelli L., Macheret S.O., Shneider M.N., Girgis I.H., Zaidi S.H., and Mansfield, D.K., "Suppression of Sonic Boom by Dynamic Off-Body Energy Addition and Shape Optimization," AIAA Paper 2002-0150

43. Zaidi S.H., Shneider M.N., Mansfield D.K., Ionikh Yu.Z., and Miles R.B., "Influence of Upstream Pulsed Energy Deposition on a Shockwave Structure in Supersonic Flow," AIAA Paper 2002-2703
44. Yan H., Adelgren R., Elliott G., Knight D., Beuthner T., and Ivanov M., "Laser Energy Deposition in Intersecting Shocks," AIAA Paper 2002-2729
45. Kandala R., and Candler G., "Numerical Studies of Laser-Induced Energy Deposition for Supersonic Flow Control," AIAA Paper 2003-1052
46. Kolesnichenko Yu., Brovkin V., Azarova O., Grudnitsky V., Lashkov V., and Mashek I., "Microwave Energy Release Regimes for Drag Reduction in Supersonic Flows," AIAA Paper 2002-0353
47. Kolesnichenko Yu., Brovkin V., Azarova O., Grudnitsky V., Lashkov V., and Mashek I., "MW Energy Deposition for Aerodynamic Application," AIAA Paper 2003-361
48. Georgievsky P.Yu., and Levin V.A., "Bow-Shock-Wave-Structure Dynamics for Pulse-Periodic Energy Input into a Supersonic Flow", 5th Int. Workshop on Magneto-Plasma Aerodynamics for Aerospace Applications, Moscow, 2003.
49. Rosa R.J., "Magnetohydrodynamic Energy Conversion," McGraw-Hill, 1968, Chap. 3, 4.
50. Macheret S. O., Shneider M. N., and Miles R. B., "Electron Beam Generated Plasmas in Hypersonic MHD Channels", AIAA Paper 99-3635, 1999.
51. Macheret S. O., Shneider M. N., and Miles R. B., "MHD Power Extraction from Cold Hypersonic Air Flow with External Ionizers", AIAA Paper 99-4800, 1999.
52. Macheret S. O., Shneider M. N., and Miles R. B., "MHD Power Extraction from Cold Hypersonic Air Flow with External Ionizers", *Journal of Propulsion and Power*, Vol. 18, No. 2, 2002, pp. 424-431.
53. Macheret S. O., Shneider M. N., Miles R. B., and Lipinski R. J., "Electron Beam Generated Plasmas in Hypersonic Magnetohydrodynamic Channels", *AIAA Journal*, 2001, Vol. 39, No. 6, pp. 1127-1136.
54. Raizer Y.P., and Shneider M.N., "Simplified Kinetic Equation for Electrons in Nonuniform Fields of Arbitrary Strength in Connection with the Cathode Sheath of a

Glow Discharge,” *Soviet Journal of Plasma Physics*, Vol. 15, No. 3, 1989, pp. 184-189.

55. Murray R.C., Zaidi S.H., Carraro M.R., Vasilyak L.M., Shneider M.N., Macheret S.O., and Miles, R.B., “Investigation of a Mach 3 Cold Air MHD Channel,” AIAA Paper 2003-4282, 34<sup>th</sup> AIAA Plasmadynamics and Lasers Conference, Orlando, FL, 23-26 June 2003.